Cellular/Molecular

Oligodendrocyte Precursor Cells Are Accurate Sensors of Local K^+ in Mature Gray Matter

Paloma P. Maldonado,[1,2,3] Mateo Vélez-Fort,[1,2,3] Françoise Levavasseur,[1,2,3] and María Cecilia Angulo[1,2,3]

[1]INSERM U603, 75006 Paris, France, [2]CNRS UMR 8154, 75006 Paris, France, and [3]Université Paris Descartes, Sorbonne Paris Cité, 75006 Paris, France

Oligodendrocyte precursor cells (OPCs) are the major source of myelinating oligodendrocytes during development. These progenitors are highly abundant at birth and persist in the adult where they are distributed throughout the brain. The large abundance of OPCs after completion of myelination challenges their unique role as progenitors in the healthy adult brain. Here we show that adult OPCs of the barrel cortex sense fine extracellular K^+ increases generated by neuronal activity, a property commonly assigned to differentiated astrocytes rather than to progenitors. Biophysical, pharmacological, and single-cell RT-PCR analyses demonstrate that this ability of OPCs establishes itself progressively through the postnatal upregulation of Kir4.1 K^+ channels. In animals with advanced cortical myelination, extracellular stimulation of layer V axons induces slow K^+ currents in OPCs, which amplitude correlates with presynaptic action potential rate. Moreover, using paired recordings, we demonstrate that the discharge of a single neuron can be detected by nearby adult OPCs, indicating that these cells are strategically located to detect local changes in extracellular K^+ concentration during physiological neuronal activity. These results identify a novel unitary neuron–OPC connection, which transmission does not rely on neurotransmitter release and appears late in development. Beyond their abundance in the mature brain, the postnatal emergence of a physiological response of OPCs to neuronal network activity supports the view that in the adult these cells are not progenitors only.

Introduction

Oligodendrocyte precursor cells (OPCs) are a class of progenitors that generate myelinating oligodendrocytes in the CNS during development and after demyelinating injury through a myelin repair process (Richardson et al., 2011). Recent Cre-Lox fate-mapping studies have also suggested that the fate of OPCs is relatively flexible, producing astrocytes and neurons in specific brain regions, although the multipotent capacity of OPCs is still a matter of intense debate (Richardson et al., 2011). In any case, OPCs have always been regarded as progenitors, even in the healthy adult brain where they constitute 2–3% of total cells in gray matter and 5–8% in white matter (Dawson et al., 2003). Nevertheless, their large abundance and widespread distribution have suggested that, in addition to their role as progenitors, OPCs reside in the mature brain to play other functions. In support of this view, a few scattered reports have shown that OPCs undergo important physiological modifications during postnatal development. In the hippocampus, the biophysical phenotype of OPCs, characterized by an outward rectifying *I–V* relationship during the two first postnatal weeks, progressively changes toward a linear shape (Kressin et al., 1995; Zhou et al., 2006). Developmental alterations in membrane receptor expression also occur in these cells. This is the case for the subunit composition of AMPA receptors (Ziskin et al., 2007; Mangin et al., 2008; Maldonado et al., 2011) and for the postnatal downregulation of nicotinic receptors (Vélez-Fort et al., 2009). Finally, complex changes have been reported concerning the mechanisms governing neuron-to-OPC communication in the brain. Glutamatergic synaptic responses of OPCs (Bergles et al., 2000; Karadottir et al., 2005; Kukley et al., 2007; Ziskin et al., 2007) increase in amplitude during the first three postnatal weeks, probably indicating a maturation process of these synapses (Ziskin et al., 2007; Mangin et al., 2008; De Biase et al., 2010). In contrast, direct GABAergic synaptic inputs of OPCs in the barrel cortex are lost early in postnatal development and replaced in the adult by an extrasynaptic mode of transmission, mediated solely by GABA spillover (Vélez-Fort et al., 2010).

Despite all these recent indications of divergent properties between young and adult OPCs, more efforts are needed to decipher developmental physiological changes that govern so far unrecognized functions of these cells in the brain. In particular, little information exists on neuron-to-OPC signaling in mature gray matter. In this report, we investigated the properties of neuron-to-OPC communication when myelination is advanced in the barrel cortex. We found that, beyond neurotransmitter transmission, adult OPCs are able to efficiently detect local $[K^+]_o$ in-

Received April 23, 2012; revised Nov. 7, 2012; accepted Dec. 7, 2012.

Author contributions: P.P.M., F.L., and M.C.A. designed research; P.P.M., M.V.-F., and M.C.A. performed research; F.L. contributed unpublished reagents/analytic tools; P.P.M. analyzed data; P.P.M., M.V.-F., and M.C.A. wrote the paper.

This work was supported by Grant R11077KK from Agence Nationale de la Recherche and Grants R09206KK and R11077KK from Fondation pour l'aide à la recherche sur la Sclérose en Plaques. P.P.M. was supported by a fellowship from Ecole des Neurosciences de Paris. M.V-F. was supported by a fellowship from Ligue Française contre la Sclérose en Plaques. We thank D.E. Bergles and F. Lesage for the gift of NG2-DsRed and TWIK1 $^{-/-}$ transgenic mice, respectively; Isabel Llano and Troy W. Margrie for helpful comments on the manuscript; E. Audinat for advice in single-cell RT-PCR and discussions; and N. Cortés, J. Montanaro, Q. Bourgeois, and the SCM Imaging Platform of the Sts-Pères Biomedical Sciences site of Paris Descartes University for technical assistance.

The authors declare no competing financial interests.

Correspondence should be addressed to Dr. María Cecilia Angulo, Laboratoire de Neurophysiologie et Nouvelles Microscopies, INSERM U603, CNRS UMR 8154, Université Paris Descartes, Sorbonne Paris Cité, 45 rue des Saints-Pères, 75006 Paris, France. E-mail: maria-cecilia.angulo@parisdescartes.fr.

M. Vélez-Fort's present address is Division of Neurophysiology, National Institute for Medical Research, Mill Hill, London NW7 1AA, United Kingdom.

DOI:10.1523/JNEUROSCI.1961-12.2013

 0270-6474/13/332432-11$15.00/0

creases generated by action potential discharges of individual cortical neurons. We also show that this process is mediated by the progressive upregulation of Kir4.1 channels in OPCs during postnatal development. The emergence of Kir4.1 channels in adult OPCs makes these cells accurate sensors of K^+ efflux during neuronal physiological activity.

Materials and Methods

Slice preparation and electrophysiology. All experiments followed European Union and institutional guidelines for the care and use of laboratory animals. Acute parasagittal slices (300 μm) of the barrel cortex were mainly performed at the 2 postnatal (PN) week and 4–5 PN weeks as previously described (Vélez-Fort et al., 2010). OPCs were identified in NG2-DsRed BAC transgenic mice (560 nm excitation and 620 nm emission wavelengths; Green OptoLed, Cairn Research). Patch-clamp recordings were performed at 33°C using an extracellular solution containing the following (in mM): 126 NaCl, 2.5 KCl, 1.25 NaH_2PO_4, 26 $NaHCO_3$, 20 glucose, 5 pyruvate, 2 $CaCl_2$, and 1 $MgCl_2$ (95% O_2, 5% CO_2). The intracellular solution was either a CsCl-based intracellular solution containing the following (in mM): 130 CsCl, 10 4AP, 5 TEA-Cl, 5 EGTA, 0.5 $CaCl_2$, 2 $MgCl_2$, 10 HEPES, 2 Na_2ATP, 0.2 Na-GTP, 10 Na_2-phosphocreatine, or a KCl-based intracellular solution containing the following (in mM): 130 KCl, 5 EGTA, 0.5 $CaCl_2$, 2 $MgCl_2$, 10 HEPES, 2 Na_2ATP, 0.2 Na-GTP, 10 Na_2-phosphocreatine (pH ~ 7.3, 296 mOsm). When isoflurane was used in the perfusion, it was dissolved in the extracellular solution immediately before its bath application at room temperature and maintained in a sealed bottle in which bubbling was stopped, as previously described (Taverna et al., 2005). Changes in $[K^+]_o$ from 2.5 to 10 mM were obtained by isotonic replacement of Na^+.

Extracellular stimulations were obtained using a monopolar electrode (glass pipette) placed in layer V of the barrel cortex (100 μs stimulations; Iso-Stim 01D, npi electronic). Paired-pulse and trains of stimulation of neurons were performed at 40 V, unless otherwise indicated. Neurons were recorded in voltage-clamp and current-clamp modes with an intracellular solution containing the following (in mM): 130 K-gluconate, 5 EGTA, 0.5 $CaCl_2$, 2 $MgCl_2$, 10 HEPES, 2 Na_2ATP, 0.2 Na-GTP, and 10 Na_2-phosphocreatine. They were held at −70 or −90 mV after correction for a liquid junction potential (10 mV). In simultaneous recordings between a neuron and an OPC, depolarizing current pulses of 200 or 400 pA were applied during 400 ms to the neuron, each 3–5 s to elicit action potential discharges. In simultaneous neuron-neuron recordings, the duration of this pulse was also increased to 800 ms, and the postsynaptic neuron was held to −90 mV as OPCs. Recordings were made without series resistance (R_s) compensation; R_s was monitored during recordings, and cells showing a change of >30% in R_s were discarded. Whole-cell recordings were obtained using Multiclamp 700B, filtered at 2–4 kHz, and digitized at 20 kHz. Digitized data were analyzed off-line using pClamp 10.1 (Molecular Devices) and Igor Pro 6.0.

Because the decay of inward K^+ currents evoked by neuronal stimulation was not well described by a single exponential function, we estimated the time required to decay by measuring the half-decay time of the current evoked by paired-pulse stimulation. The paired-pulse ratio of these currents was obtained by dividing the current amplitude of the second pulse by that of the first pulse. In simultaneous patch-clamp recordings, currents evoked in OPCs by single neuron firing were considered as a response only if they were on average larger than 2 times the SD of noise and if their amplitude distribution was significantly different from that of the noise.

Steady-state *I–V* curves were obtained by applying voltage steps of 400 ms from +40 mV to −140 mV and by measuring current amplitudes at 390 ms from the beginning of the steps. It is noteworthy that we already showed that neither the capacitance nor the morphology of OPCs of the barrel cortex changes during development (Vélez-Fort et al., 2010). *I–V* curves of currents sensitive to different agents were obtained by subtracting currents in the presence of a drug from their controls and normalizing with respect to the current elicited at +40 mV in control. To determine the percentage of OPCs having a young phenotype in 4–5PN weeks, we plotted the distribution of current amplitudes elicited at a voltage step of +40 mV in all recorded cells of the 2PN week. In the distribution graph, 90% of OPCs had a current amplitude inferior to 420 pA, which corresponds to the mean current amplitude plus the SD (mean ± SD: 220 ± 198; $n = 26$). We thus considered as a young phenotype all cells having a current <420 pA and as an adult phenotype those having currents >420 pA at a voltage step of +40 mV. Only cells recorded in the CsCl-based intracellular solution with an adult phenotype were considered for analysis (70% of OPCs in 4–5PN weeks).

Immunohistochemistry. For MBP and vGluT2 immunostainings, mice were perfused intracardially with PBS alone followed by 0.15 M phosphate buffer, pH 7.4 (PB) containing 4% paraformaldehyde at PN7, PN13–14, and PN27–31 ($n = 3$ animals for each developmental stage). Brains were removed and placed in a 4% paraformaldehyde solution overnight. Then, brain slices (50 μm) were prepared in PBS ice-cold solution (4°C), permeabilized with 1% Triton X-100 and 2% BSA for 1 h, and incubated two nights with antibodies diluted in a 0.2% Triton X-100 solution. Double immunostainings were performed by combining guinea pig polyclonal vGluT2 (1:1000; Millipore) with mouse monoclonal anti-MBP (1:100; Millipore). Primary antibodies were washed three times in PBS and incubated in secondary antibodies coupled to Alexa Fluor 488 or Alexa Fluor 633 (1:500; Invitrogen) for 2 h at room temperature.

For simultaneous recordings between neurons and OPCs, recorded cells were injected with 5.4 mM biocytin (Sigma-Aldrich). The slices containing the injected cells were then fixed overnight in 4% paraformaldehyde at 4°C, rinsed three times in PBS for 10 min, and incubated with 1% Triton X-100 and 2% BSA during 1 h. The slices were incubated overnight with rabbit polyclonal anti-NG2 antibody (1:400; Millipore) diluted in a 0.2% Triton X-100 solution. Then, they were washed three times in PBS and incubated in the secondary antibody coupled to Alexa Fluor 633 and streptavidin–Alexa Fluor 488 (Invitrogen) for 2 h.

Immunofluorescence was visualized with a confocal microscope (LSM 510, Carl Zeiss). Optical sections of confocal images were sequentially acquired using a 10× or 63× oil objectives (NA = 0.3 and 1.4, respectively) with the LSM-510 software. Images were processed and analyzed using ImageJ 1.44c (Wayne Rasband, National Institutes of Health). Because cortical layer I were poorly myelinated, we eliminated the background noise of MBP immunostainings by subtracting the fluorescence intensity of this layer to the whole image.

Single-cell RT-PCR and genotyping of NG2-DsRed::TWIK1 $^{-/-}$ transgenic mice. The analysis of single-cell transcripts for Kir4.1 channels was performed as previously described with modifications (Angulo et al., 1997; Seifert et al., 2009). Briefly, we harvested the cytoplasm of recorded cells with a patch pipette filled with 6 μl of an autoclaved DEPC-treated internal solution containing the following (in mM): 130 CsCl, 5 4-AP, 10 TEA-Cl, 2 $MgCl_2$, 0.2 EGTA, and 10 HEPES, pH 7.4, 290 mOsm. The content of the pipette was expelled into a test tube, and the reverse transcription (RT) was performed for 2 h at 50°C in a 10 μl reaction volume by adding the following components at final concentrations as indicated: 10 ng/μl hexamer random primers, 0.5 mM each dNTP, 5 mM DTT, 20 U of RNaseOut (Invitrogen), 100 U of Superscript III Reverse Transcriptase (Invitrogen), and 1× buffer supplied with the enzyme. After incubation, the tubes were kept at −20°C. The RT products were then amplified with primers for a two-round nested PCR (Seifert et al., 2009). The first PCR was done for 35 cycles (94°C, 30 s; 54°C, 30 s; 72°C, 45 s) after adding Taq polymerase (2.5 U; QIAGEN), 1× buffer supplied by the manufacturer, 100 μM dNTP, and the following primers (0.3 μM each): 5′ TATCAGAGCAGCCACTTCACCTTC 3′ and 5′ GGATCGTCTCGGCCCTCTTCTTAG 3′ (final volume, 100 μl). An aliquot of 1.5 μl of the PCR product was then used as a template for the second PCR (35 cycles; 94°C, 30 s; 58°C, 30 s; 72°C, 30 s) performed with the following nested primers: 5′ TTCACCTTCGAGCCAAGATGACG 3′ and 5′ AGGCGTGTGGTTGGCAGGAG 3′ (final volume, 25 μl). The positive control consisted of running in parallel RT-PCR for single cells and for total RNA (50 pg) from mouse hippocampus. Two negative controls were obtained by running RT-PCR either after omitting RT or for harvested cortical layer I-III neurons.

NG2-DsRed::TWIK1 $^{+/-}$ animals were generated by crossing heterozygous NG2-DsRed mice with homozygous TWIK1 knock-out

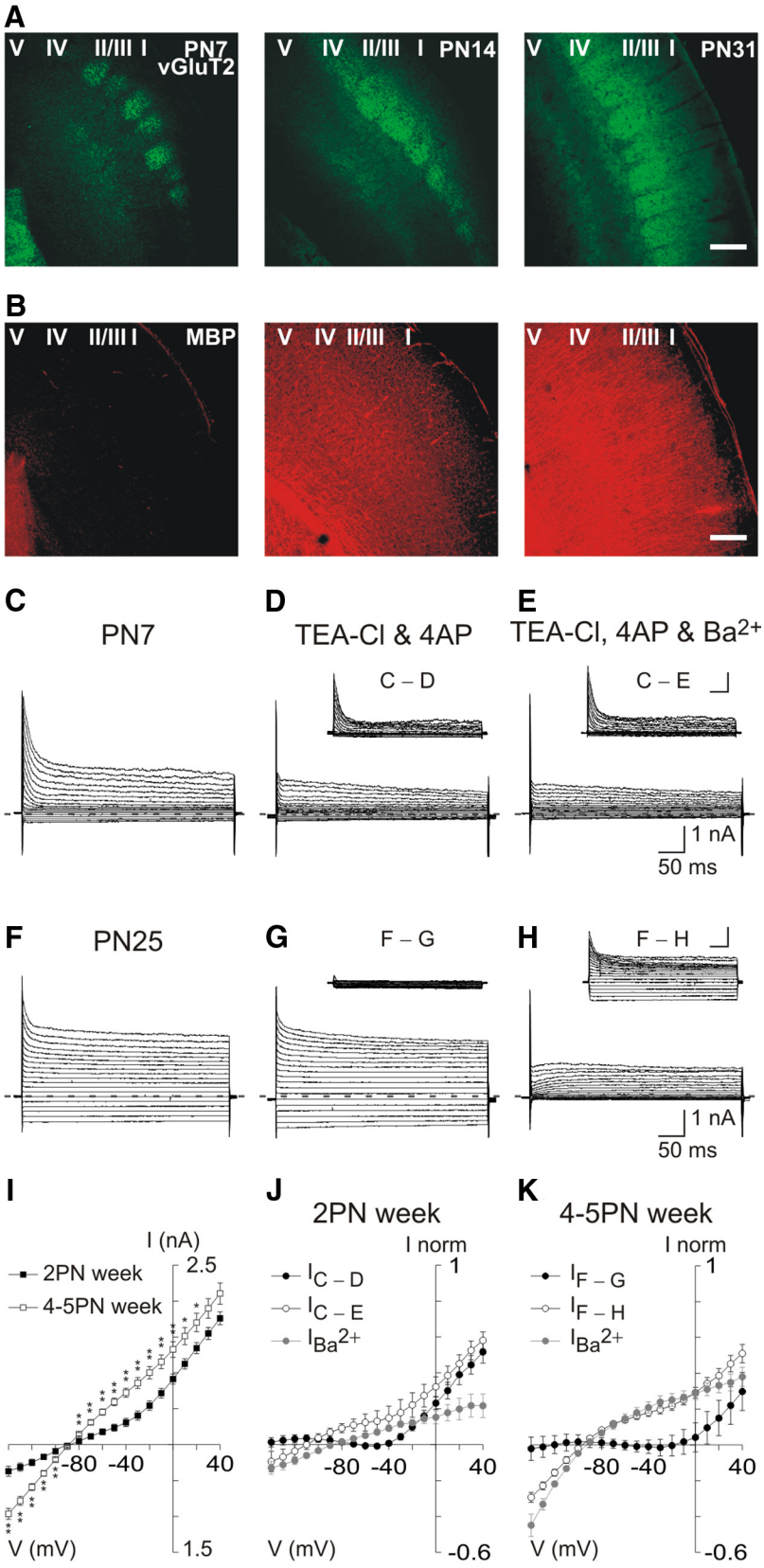

Figure 1. Cortical OPCs acquire a linear electrophysiological phenotype during postnatal myelination of the barrel cortex. ***A***, ***B***, Confocal images of a double immunostaining against the vesicular transporter for glutamate vGluT2 and the MBP at PN7, PN13–14, and PN27–31 (objective 10×; 1 optical section of 12.5 μm). vGluT2 immunoreactivity is enriched in barrel structures of layer IV (***A***). Note that cortical myelination starts in the 2PN week and is already advanced at 4–5PN weeks (***B***). Scale bar, 200 μm. ***C–H***, Currents induced in two OPCs held at −90 mV at PN7 (***C–E***) and PN25 (***F–H***) by voltage steps from +40 mV to −140 mV, using a KCl-based intracellular solution, in control conditions (***C***, ***F***), after adding in the bath 10 mM TEA and 4 mM 4AP (***D***, ***G***), and 10 mM TEA, 4 mM 4AP, and 100 μM Ba^{2+} (***E***, ***H***). Hyphenated gray lines correspond to zero current for all cases. Insets show subtracted currents with respect to controls. Calibration: 1 nA, 50 ms. ***I***, Comparison of steady-state *I–V* curves in control conditions between the 2PN and 4–5PN weeks ($n = 16$ and $n = 42$, respectively). Note that the outward rectification in the 2PN week changes to a linear shape in 4–5PN weeks. *$p < 0.05$. **$p < 0.01$. ***J***, ***K***, Comparison of steady-state *I–V* curves of currents sensitive to the large-spectrum K^+ channel blockers TEA, 4AP, and Ba^{2+} in the 2PN (***J***) and 4–5PN (***K***) weeks. Note that, in the 2PN week (***J***), a large outward TEA, 4AP-sensitive component (●, $n = 7$, $p < 0.05$ from −20 to +40 mV) does not significantly change after adding Ba^{2+} in the bath (○, $n = 7$, $p > 0.05$ for all potentials), and is larger than that obtained when Ba^{2+} is applied alone (gray circles, $n = 6$, $p < 0.05$ from 0 to +40 mV). In contrast, in 4–5PN weeks (***K***), a smaller TEA, 4AP-sensitive component exists (●, $n = 10$, $p < 0.05$ only for +40 mV), compared with a large Ba^{2+}-sensitive component present after adding Ba^{2+} in the bath (○, $n = 12$; $p < 0.001$ for all potentials except for −90 mV and −100 mV) or when Ba^{2+} is applied alone (gray circles, $n = 6$; $p < 0.05$ for all potentials except for −90 mV). Note that the Ba^{2+}-sensitive component is characterized by a weak inward rectification.

mice. Heterozygous double-transgenic mice were then crossed with TWIK1 $^{-/-}$ mice to obtain TWIK1 $^{-/-}$ mice expressing DsRed in littermates. This last generation was genotyped by PCR with primers designed to amplify a 434 bp and a 600 bp fragment for wild-type and knock-out sequences, respectively. PCR was done for 40 cycles (94°C, 30 s; 55.4°C, 30 s; 72°C, 1 min 30 s) with the following primers: 5′ TCCTTCCTACCGACAGCGAGAGA 3′ and 5′ GGGATGCCGATGACAGAGTAGAT 3′ for wild-type; 5′ TGCCTTTACGGTGTCTGT TC 3′ and 5′ GAGAAGGCAGAAATGGAAAC TG 3′ for knock-out. After patch-clamp experiments, we confirmed that killed animals were TWIK1 $^{-/-}$ by PCR.

Statistics. Data are expressed as mean ± SEM The nonparametric Mann–Whitney *U* test for independent samples was used to determine statistical differences between data obtained in different cells. Comparisons within single cells were performed with the Wilcoxon signed-rank test for related samples when $n \geq 6$; otherwise, we used a paired *t* test (GraphPad InStat software, Version 3.06). Amplitude distributions of induced currents in simultaneous recordings were compared using the Kolmogorov–Smirnov test (http://www.physics.csbsju.edu/stats).

Results

OPCs acquire a linear phenotype during postnatal development of the barrel cortex

The properties of OPCs of the barrel cortex during postnatal development were examined in layer V DsRed $^+$ cells recorded during 2PN and 4–5PN weeks in NG2-DsRed transgenic mice (Ziskin et al., 2007). These developmental stages were chosen to cover the critical period of

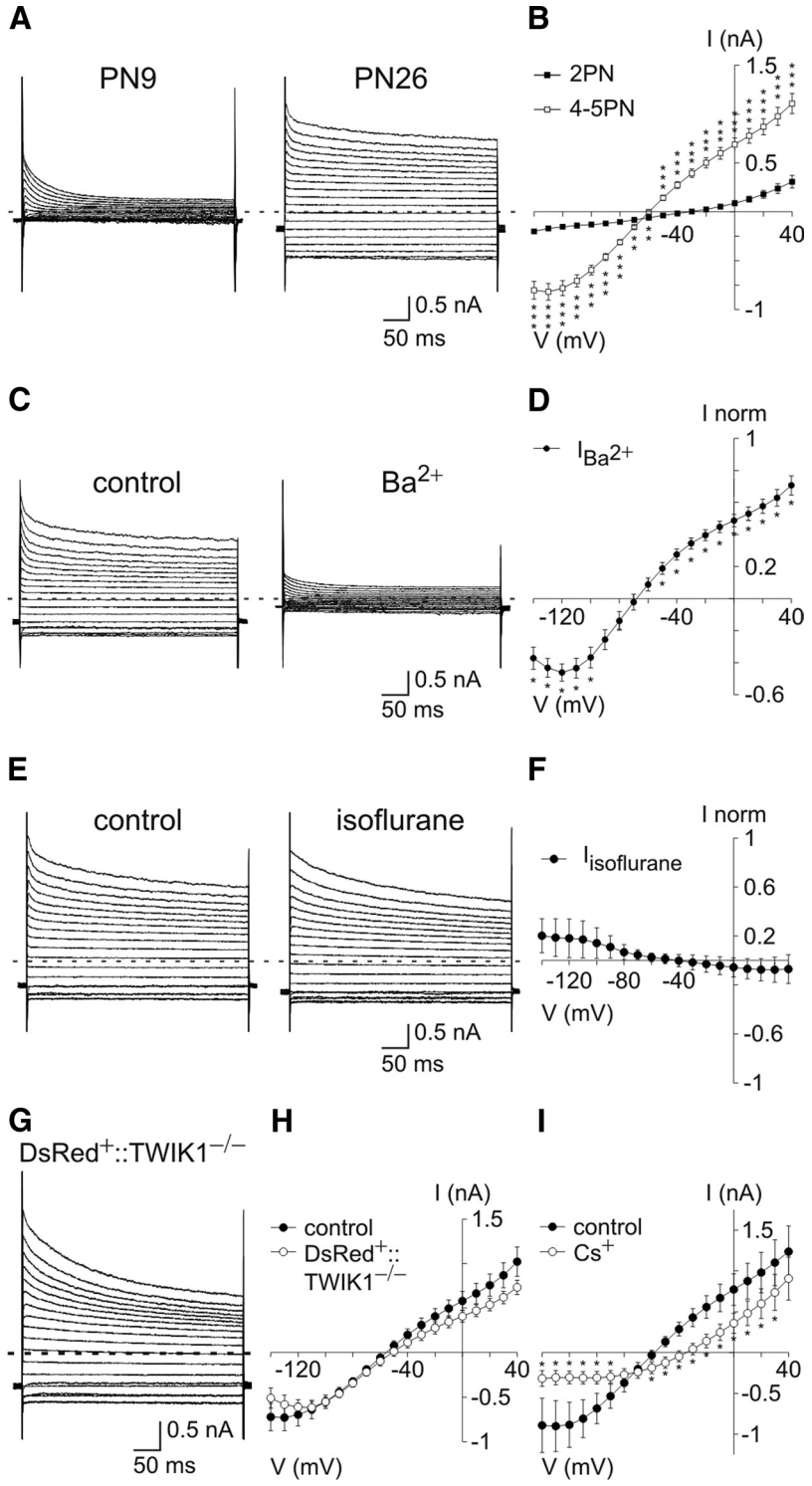

Figure 2. TWIK1 and TREK1 two-pore domain K^+ channels are not major conductances in adult OPCs. ***A***, Currents induced in OPCs held at −90 mV at PN9 and PN26 by voltage steps from +40 mV to −140 mV, using a CsCl-based intracellular solution containing TEA and 4AP. The same holding potential, voltage steps, and intracellular solution were used for the experiments below; hyphenated gray lines indicate zero current for all cases. ***B***, Steady-state mean *I–V* curves of OPCs between the 2PN ($n = 26$) and 4–5PN weeks ($n = 35$). Note the large component present only in OPCs of 4–5PN weeks. $^{**}p < 0.01$. $^{***}p < 0.001$. It is noteworthy that Na^+ currents were always observed in OPCs of 2PN week, but they are not visible with the time scale of 400 ms (see also Maldonado et al., 2011). ***C***, Currents induced in an OPC before (left) and after (right) bath application of 100 μM Ba^{2+}. ***D***, Mean steady-state *I–V* curves of currents sensitive to 100 μM Ba^{2+} ($n = 6$). $^*p < 0.05$. ***E***, Currents induced in an OPC before and after bath application of 10 mM isoflurane, a volatile anesthetic enhancing the opening of TREK1 channels (Patel et al., 1999). ***F***, Mean *I–V* curve of currents sensitive to 10 mM isoflurane. Note the lack of effect of this agent ($n = 8$). $p > 0.05$. It is also noteworthy that the acidification of intracellular medium known to increase TREK1-mediated currents (Lotshaw, 2007) instead reduced K^+ currents of OPCs (Fig. 3*B*,*D*). ***G***, Currents of OPCs in a double-transgenic NG2-DsRed::TWIK1 $^{-/-}$ mice. Because no specific pharmacological tools allowing for the unambiguous discrimination of TWIK1-mediated currents exist, these double-transgenic mice were generated to identify DsRed $^+$ OPCs in a context in which TWIK1 was inactivated (Materials and Methods). ***H***, Mean *I–V* curves of OPCs in control and NG2-DsRed::TWIK1 $^{-/-}$ mice. OPCs of NG2-DsRed::TWIK1 $^{-/-}$ mice had the same current amplitudes as those recorded in controls performed during the same period ($n = 10$ and $n = 13$, respectively). $p > 0.05$, for all potentials. ***I***, Mean *I–V* curves of OPCs in control and after bath application of 1 mM Cs^+. Note that extracellular Cs^+ abolishes most inward than outward currents ($n = 6$). $^*p < 0.05$.

myelination of deep layers of the barrel cortex (Fig. 1*A*,*B*). Indeed, cortical myelination starts in the 2PN week and is already advanced at PN30 (Fig. 1*B*), when the conduction velocity of action potentials of the thalamocortical pathway reaches a plateau (Salami et al., 2003) and intracortical circuits are relatively mature (Angulo et al., 1999; Morales et al., 2002).

OPCs were first recorded with a KCl-based intracellular solution and held at −90 mV. Application of voltage pulses from +40 mV to −140 mV revealed a dramatic developmental change in the *I–V* relationship. Comparison of steady-state *I–V* curves showed that the outward rectification observed in the 2PN week changes to a linear shape in 4–5PN weeks (Fig. 1*C*,*F*,*I*). This modification of the ion current profile was observed at least until PN54 ($n = 4$) and was accompanied by a more hyperpolarized resting membrane potential (−77.9 ± 2.7 mV in the 2 PN week vs −88.1 ± 2.5 mV in 4–5PN weeks, respectively; $p < 0.01$) and a decreased input resistance (281.8 ± 59.7 MΩ in the 2PN week against 70.9 ± 6.5 MΩ in the 4–5PN weeks, respectively; $p < 0.001$).

The sensitivity of currents evoked by voltage steps to the large-spectrum K^+ channel blockers TEA and 4AP was also different between both developmental stages. These antagonists blocked a large proportion of outward currents in the 2PN week (Fig. 1*D*,*J*) but affected to a smaller extent those in the 4–5PN weeks (Fig. 1*G*,*K*). In contrast, a subsequent application of Ba^{2+} inhibited modestly additional currents in young mice (Fig. 1*E*,*J*) but suppressed substantial currents in older mice (Fig. 1*H*,*K*). This is consistent with the effect of Ba^{2+} applied alone. Small Ba^{2+}-sensitive currents were revealed in the 2PN week (Fig. 1*J*), whereas large currents had similar amplitudes than those recorded in the presence of TEA, 4AP, and Ba^{2+} in 4–5PN weeks (Fig. 1*K*).

These results indicate that a Ba^{2+}-sensitive, TEA-insensitive, and 4AP-

insensitive conductance, the identity of which is unknown, is upregulated in OPCs during postnatal development of the barrel cortex. The weakly inward rectification of this conductance counteracts the outward rectification observed in the 2PN week, conferring a linear phenotype on OPCs in the adult (Fig. 1*I*,*K*).

Identification of Kir4.1 channels as a major postnatal upregulated conductance in OPCs

The emergence of a linear *I–V* curve has been previously described in hippocampal OPCs (Kressin et al., 1995; Zhou et al., 2006), but the conductance conferring a linear phenotype in the adult has not been identified yet. To isolate the Ba^{2+}-sensitive current upregulated in OPCs, we tested a CsCl-based intracellular solution containing TEA and 4AP, known to suppress from the inside most currents mediated by voltage-gated K^+ channels. This solution almost completely abolished intrinsic currents in young mice, whereas significant currents still remained in 70% of OPCs of 4–5PN weeks (considered as OPCs with an adult phenotype; see Materials and Methods; Fig. 2*A*,*B*). Furthermore, bath application of 100 μM Ba^{2+} almost completely blocked currents of intrinsic *I–V* curves in adult OPCs (Fig. 2*C*,*D*), indicating that this intracellular solution is convenient to block voltage-gated K^+ channels and isolate the currents of our interest.

To identify the K^+ conductance postnatally upregulated in OPCs, we examined the effect of different blockers for K^+ channels insensitive to TEA and 4AP and sensitive to Ba^{2+} (i.e., small-conductance Ca^{2+}-activated potassium [SK] channels) (Sah and Faber, 2002), the two-pore domain K^+ channels TREK1 and TWIK1 (Lesage et al., 1996; Lotshaw, 2007), and inwardly rectifying (Kir) channels (Hibino et al., 2010). First, we excluded the contribution of SK channels in OPCs of 4–5PN weeks by applying their selective antagonist apamin and detecting no effects on the recorded currents (200 nM; $p > 0.05$; $n = 5$) (Sah and Faber, 2002). Then, we examined whether TWIK1 and TREK1 were functionally expressed. According to a transcriptome database, the mRNAs of the two-pore domain K^+ channels TWIK1 and TREK1 are preferentially enriched in acutely isolated purified OPCs (Cahoy et al., 2008). However, the lack of effect of isoflurane in these currents, an anesthetic activating TREK1 (Fig. 2*E*,*F*), and the unchanged electrophysiological phenotype of OPCs in a transgenic mouse expressing inactivated TWIK1 (Fig. 2*G*,*H*) (Nie et al., 2005) show that, contrary to astrocytes (Seifert et al., 2009; Zhou et al., 2009), two-pore domain K^+ channels are poorly expressed in adult OPCs.

It is well known that Cs^+ blocks Kir channels from the outside in a voltage-dependent manner (Hibino et al., 2010; Tang et al., 2010). In a CsCl-based intracellular solution, bath applications of 1 mM Cs^+ blocked currents of the *I–V* curve from the outside as expected for Kir channels (i.e., abolishing most inward currents and only weakly outward currents; Fig. 2*I*) (Hibino et al., 2010; Tang et al., 2010). Although the effect of intracellular Cs^+ is poorly characterized for Kir channels, some effect was evident because currents, particularly inward currents, appeared reduced compared with those recorded in KCl-based intracellular solution (Fig. 2*B* for CsCl vs Fig. 1*I* for KCl) and E_{rev} was shifted from -88.14 ± 2.46 mV to -59.30 ± 1.30 mV ($p < 0.001$). These data strongly suggest a major expression of a Kir conductance in adult OPCs. In support of this and as mentioned above, 100 μM Ba^{2+}, a well-known Kir blocker at this concentration (Hibino et al., 2010), abolished currents of intrinsic *I–V* curves in adult OPCs (Fig. 2*C*,*D*).

Among Kir channels, Kir4.1 channels are found almost exclusively in glial cells (Poopalasundaram et al., 2000; Higashi et al., 2001; Seifert et al., 2009; Tang et al., 2009). Because the deletion of Kir4.1 channels in transgenic mice is lethal around the end of the third PN week (Kofuji et al., 2000; Djukic et al., 2007), we used pharmacological tools to examine its functional expression in OPCs of the 4–5PN weeks. First, we assessed the effect of the tricyclic antidepressant desipramine, an inhibitor of Kir4.1 currents that affects only slightly other Kir currents in heterologous expression systems (Su et al., 2007). In adult OPCs recorded in CsCl-based intracellular solution, this agent almost completely abolished K^+ currents (Fig. 3*A*,*C*). Previous works also demonstrated a partial sensitivity of Kir4.1 channels to an intracellular pH of 6.5 (Tucker et al., 2000; Pessia et al., 2001). To test for the effect of acidic pH, we performed two consecutive whole-cell patch-clamp recordings on the same cell with intracellular solutions at pH of 7.4 and 6.3, respectively (Fig. 3*B*,*D*). We observed a decrease of current amplitudes to voltage steps during the second whole-cell recording, an effect compatible to the acidic pH sensitivity reported for homomeric Kir4.1 channels (reduction of $51.0 \pm 5.9\%$ at +40 mV; Fig. 3*D*) (Tucker et al., 2000; Pessia et al., 2001). To verify that this effect was not caused by degradation of the cell by removing the first patch pipette, we performed the same experiments without changing the pH during the second whole-cell recording. In that case, no changes on the *I–V* relationship were observed, confirming the effect of acidic pH (Fig. 3*D*, black circles). Finally, we performed single-cell nested RT-PCR experiments to detect transcripts for Kir4.1 channels in OPCs of the barrel cortex (Fig. 3*E*; see Materials and Methods). Kir4.1 transcripts were found in 7 of 9 recorded adult OPCs (78%), whereas they were amplified in only 1 of 10 cortical neurons (10%). Biophysical, pharmacological, and molecular analyses indicate that Kir4.1 channels are by far the major K^+ conductance developmentally upregulated in OPCs of the mature barrel cortex and that this conductance contribute to the linear phenotype of *I–V* relationships in the adult.

Adult OPCs detect local K^+ increases through upregulated Kir4.1 channels

Astrocytes are accurate detectors of neuronal activity through a Kir4.1 conductance (De Saint Jan and Westbrook, 2005; Djukic et al., 2007). Because Kir4.1 channels are postnatally upregulated in OPCs, we tested whether, similarly to astrocytes, these cells are able to sense extracellular $[K^+]_o$ increases through these channels in the mature neuronal network. For this, an extracellular electrode placed in layer V was used to stimulate neuronal fibers while $NG2^+$/$DsRed^+$ OPCs were recorded at −70 mV with the CsCl-based intracellular solution to accurately isolate Kir4.1-mediated currents (Fig. 4*A*,*B*). Experiments in older mice were performed in OPCs having an adult phenotype. Paired-pulse stimulation easily elicited currents in OPCs of the 2PN and 4–5PN weeks (mean amplitude of first pulse: -136.8 ± 41.5 pA and -159.5 ± 45.0 pA; $n = 8$ and $n = 13$, respectively; Fig. 4*C*,*D*, gray traces) (Vélez-Fort et al., 2010). However, whereas the ionotropic glutamatergic and GABAergic receptor antagonists in young mice abolished these currents, a persistent current remained in older mice ($1.7 \pm 0.6\%$ and $17.7 \pm 4.4\%$ in 2PN and 4–5PN weeks, respectively; $p < 0.001$; Fig. 4*C*,*D*, black traces). This persistent current in older mice was characterized by long-lasting kinetics with a half-decay time of 0.45 ± 0.03 s and a much weaker paired-pulse depression compared with control conditions (paired-pulse ratio of 0.93 ± 0.03 in antagonists against 0.22 ± 0.03 in controls, $n = 13$; $p < 0.001$; see Materials and Methods). Moreover, its amplitude increased an average when the stimulation intensity varied from 20 to 40 V (increment of 70.1%; $n = 13$ and $n = 23$, respectively; $p < 0.01$) or when trains

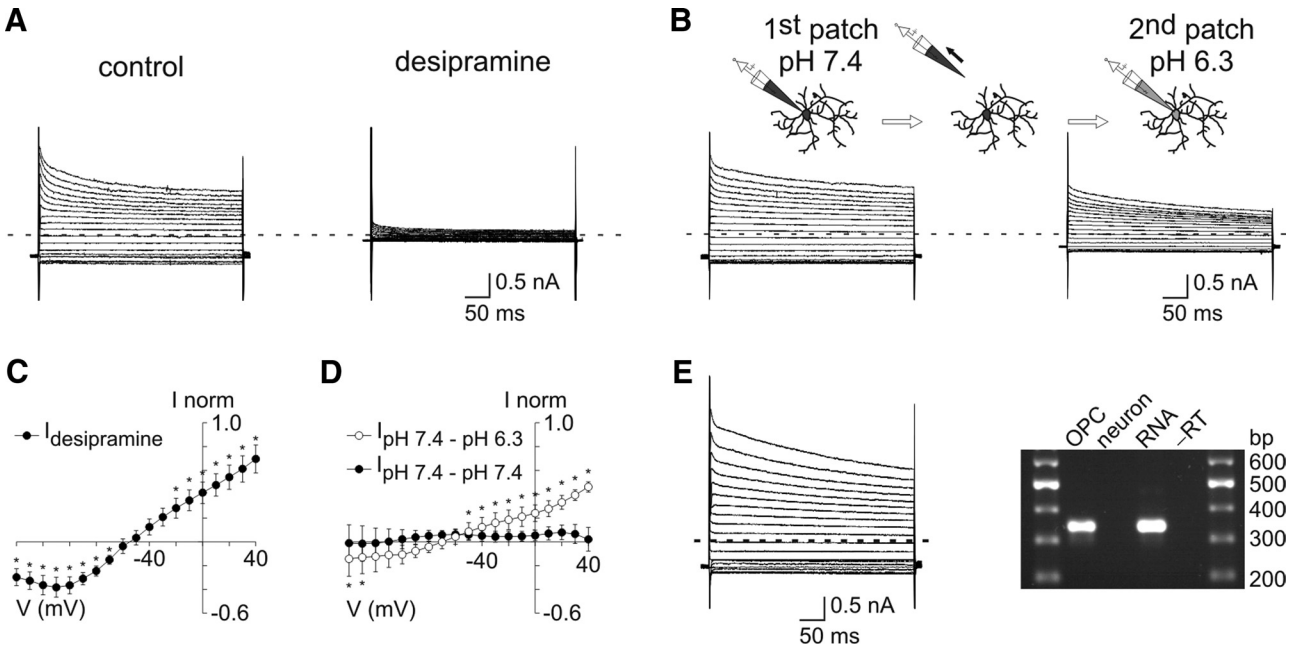

Figure 3. Kir4.1 channels are upregulated in OPCs of the mature barrel cortex. ***A***, ***C***, Effect of 100 μM desipramine on currents induced in an OPC using a CsCl-based intracellular solution containing TEA and 4AP and held at −90 mV by voltage steps from +40 mV to −140 mV in 4–5PN weeks. The mean steady-state *I–V* curve shows currents sensitive to desipramine (***C***) ($n = 6$). *$p < 0.05$. The same holding potential and voltage steps were used for the experiments below; and hyphenated gray lines indicate zero current for all cases. ***B***, ***D***, Effect of intracellular acidification on currents induced in OPCs in 4–5PN weeks. As shown in the diagram (top), two consecutive patches were performed in the same cell with CsCl-based intracellular solutions at a pH of 7.4 and of 6.3. Mean steady-state *I–V* curves were obtained by subtracting current traces of the second patch from those of the first patch (***D***) (○; $n = 7$). *$p < 0.05$. As a control, the same experiment was performed without changing the pH during the second whole-cell recording (***D***) (●; $n = 4$). $p > 0.05$ for all potentials. ***E***, Currents induced in OPCs at PN23 (left) and analyzed by single-cell RT-PCR (right). After recording, the cytoplasm was harvested and nested RT-PCR for the Kir4.1 channel was performed. Kir4.1 was expressed in this OPC as shown in the agarose gel (338 bp; right). Note that the control of total RNA (RNA; 50 pg) was positive, whereas either a neuron or the negative control without RT (−RT) was not.

of stimuli were applied (50 Hz; peak amplitude: −207.61 ± 59.7 pA; $n = 5$; Fig. 4*F*). In contrast, even at high rates of stimulation, the persistent current was negligible in OPCs of the 2PN week (50 Hz; peak amplitude: −10.1 ± 4.5 pA; $n = 8$; Fig. 4*E*). In older animals, the supplement in the antagonist solution of metabotropic glutamatergic and GABAergic receptor blockers LY341495 (50 μM) and CPG55845 (5 μM) and of the purinergic receptor blocker PPADS (30 μM) were without effect, indicating that the persistent current in 4–5PN weeks is not mediated by common ionotropic and metabotropic receptors ($n = 4$; $p > 0.05$, Fig. 4*G*). Yet, it was completely abolished by the Na^+ channel blocker TTX, showing that it is induced by neuronal activity (88.6 ± 11.7% of block; $n = 4$; Fig. 4*H*). Because this current is not mediated by common neurotransmitter receptors, it probably reflects a K^+ efflux from neurons during action potential discharges as it has been described previously for astrocytes (De Saint Jan and Westbrook, 2005). Because the amplitude and kinetics of persistent currents in OPCs vary with the intensity and frequency of neuronal stimulation, the response of OPCs is able to follow different regimens of neuronal activity.

The emergence of a resistant current during development was concomitant with the upregulation of Kir4.1 channels. To analyze whether Kir4.1 channels mediated this current, we used the same pharmacological tools as described previously (Fig. 3). First, neuronal-evoked inward currents were reduced by the Kir channel blocker Ba^{2+} (71.0 ± 8.2% reduction; $n = 6$; $p < 0.05$; Fig. 5*A*). A similar effect of Ba^{2+} was seen when recording OPCs with a KCl-based intracellular solution, confirming that these Ba^{2+}-sensitive currents are evoked in physiological K^+ concentrations (91.0 ± 7.0% reduction; $n = 6$; $p < 0.05$; Fig. 5*B*). Because desipramine reduced the amplitude of synaptic currents in postsynaptic recorded neurons (reduction of 51.4 ± 14.1%; $n = 9$; $p < 0.05$), we could not use this drug. Instead, we attempted to decrease the inward K^+ current evoked by neuronal stimulation from the inside with the acidic intracellular solution. As expected for Kir4.1 channels and in agreement with our results on intrinsic *I–V* curves (Fig. 3), we obtained that the persistent inward current was significantly reduced in adult OPCs recorded at a pH of 6.3 compared with controls performed at a physiological pH, in the same slices and with the same stimulation electrodes (reduction of 50.5%, $n = 13$ and $n = 11$, respectively; $p < 0.01$; Fig. 5*C*).

If persistent inward currents reflect a transient $[K^+]_o$ rise caused by action potential discharges, their *I–V* curve should be shifted toward more positive potentials. To assess the *I–V* curve of neuronal-evoked inward currents resistant to antagonists, we performed 100 ms ramps from +40 mV to −140 mV before the stimulation and at the peak of the second response (Fig. 6*A*). As expected for a K^+ conductance, E_{rev} shifted to a more depolarized potential in all tested cells during stimulation (shift of 4.3 ± 1.2 mV; $n = 5$; $p < 0.05$; Fig. 6*B*), a value below that obtained in intrinsic *I–V* curves when $[K^+]_o$ was artificially raised to 10 mM (shift of 8.7 ± 2.3 mV; $n = 6$; $p < 0.05$; Fig. 6*C*,*D*). Therefore, neuronal stimulation induces a K^+ current in OPCs that reflects a K^+ efflux from neurons comprised between 2.5 and 10 mM as expected for physiological rates of action potential discharges (Heinemann and Lux, 1977; Kofuji and Newman, 2004).

Our data reveal that, in addition to respond to neurotransmitter release, OPCs acquire the ability during postnatal development to detect transient $[K^+]_o$ increases caused by neuronal activity via the postnatal upregulation of Kir4.1 channels. These results add a further complexity to the mechanisms governing neuron–OPC communication in the mature brain.

OPCs are accurate sensors of K^+ increases generated by single nearby neurons

To test whether adult OPCs are able to sense fine $[K^+]_o$ increases of single nearby neurons when they discharge action potentials, we performed simultaneous patch-clamp recordings between a neuron and an OPC, which somata were separated by <18 μm (range, 0–18 μm). Figure 7*A* illustrates a labeled neuron and $NG2^+$/$DsRed^+$ OPCs recorded with intracellular solutions containing biocytin. Depolarizing current pulses of 400 ms were elicited in the recorded neuron to induce action potential firing while recording the nearby OPC with a KCl-based intracellular solution (in physiological K^+ concentrations) (Fig. 7*A*, right, and 7*B*). For 21 of 26 simultaneous recordings, a train of action potentials in the neuron elicited a current in the OPC that had a mean peak amplitude of −3.1 ± 0.5 pA and showed always an amplitude distribution significantly different to that of the noise (Fig. 7*B*,*E*). Neurons eliciting a response in OPCs showed variable discharge frequencies ranging from 27.5 to 121.8 Hz, which includes pyramidal cells and interneurons, indicating that the OPC current is not induced by a specific neuronal cell type (mean frequency, 70.3 ± 15.9 Hz). It is noteworthy that neither the frequency nor the distance between cell somata where correlated to the amplitude of the current ($p > 0.05$). In addition, despite the presence of a large repertoire of K^+ channels in neurons, such current was never observed in simultaneous recordings between two neurons which somata were separated by <13 μm (range, 1–13 μm), even when the depolarizing pulse duration was increased to 800 ms (mean amplitude: −0.35 ± 0.35 pA; $n = 7$; Fig. 7*G*).

It is known that OPCs detect neuronal activity through synaptic and extrasynaptic signaling mechanisms dependent on neurotransmitter release (Maldonado et al., 2011). However, the current elicited in OPCs by single neuron stimulation was insensitive to metabotropic and ionotropic glutamate, GABA, and purinergic receptor antagonists; thus, it did not result from either classical synaptic transmission or spillover of neurotransmitters (−3.2 ± 1.0 pA and −3.4 ± 1.0 pA in control and all antagonists, respectively; $p > 0.05$; $n = 5$; Fig. 7*C*,*F*). This current developed progressively during neuronal firing without evidence of postsynaptic events, suggesting a nonsynaptic nature of the response (Fig. 7*B*,*C*). Nevertheless, considering that OPCs have a relatively low input resistance in KCl-based intracellular solution (~70 MΩ), we cannot completely exclude that the current recorded in the OPC results from an artifactual detection through the patch pipette of the depolarizing current injected to the neuron. To discard this possibility, we hyperpolarized the neuron to prevent action potential dis-

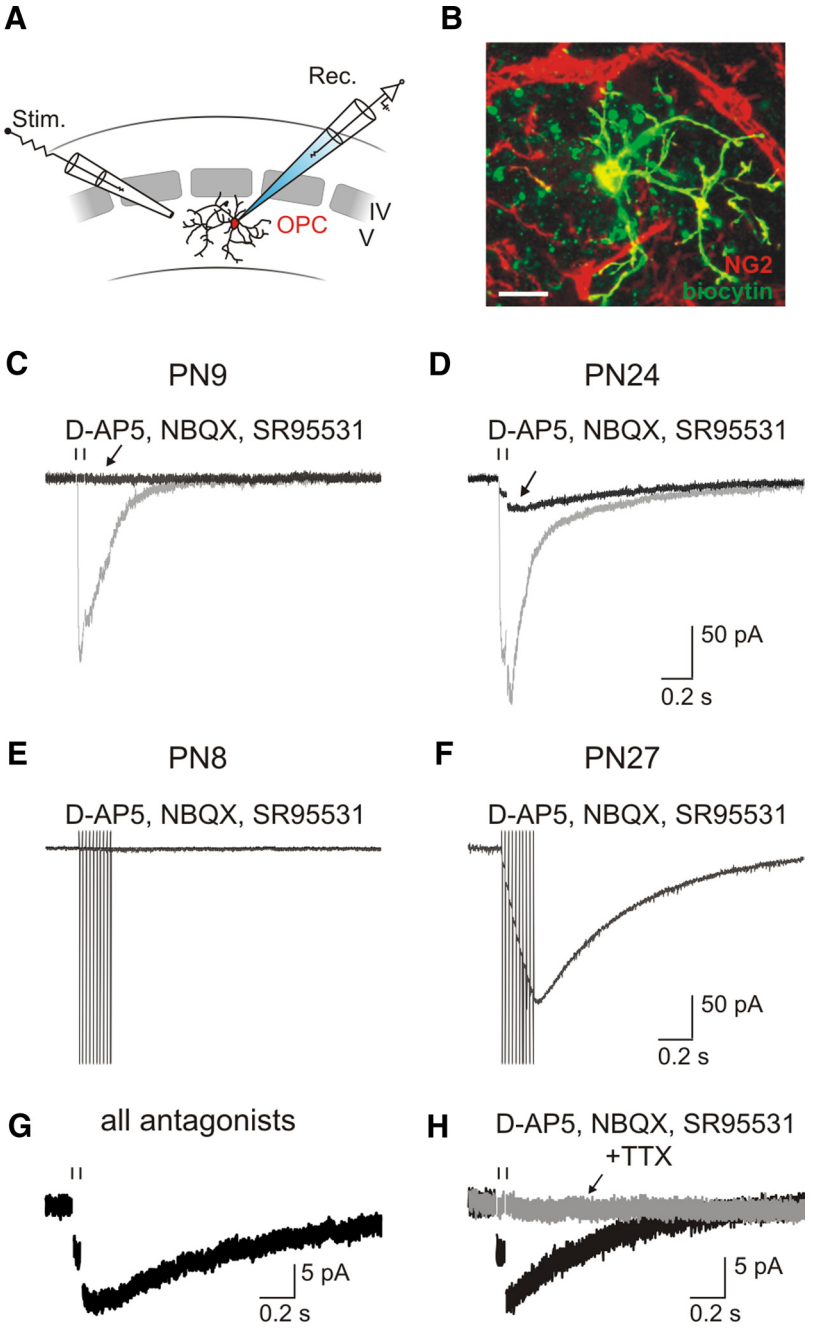

Figure 4. OPCs sense local increases of $[K^+]_o$ during neuronal activity in the mature barrel cortex. ***A***, Schematic representation of extracellular stimulation of layer V neuronal fibers during patch-clamp recordings of OPCs of the barrel cortex. ***B***, Confocal image of an $NG2^+$/$DsRed^+$ OPC recorded with an intracellular solution containing biocytin at PN24 (objective 63×; stack of 18 *z* section, each 1 μm, see Materials and Methods). Scale bar, 15 μm. ***C***, ***D***, Paired-pulse stimulation of neuronal fibers elicited inward currents in two OPCs held at −70 mV at PN9 (***C***) and PN24 (***D***) (gray traces; pulses separated by 50 ms; 100 μs, 40 V). Although the evoked current was completely abolished by 10 μM NBQX, 50 μM D-AP5, and 5 μM SR95531 in ***C***, a persistent current remained in ***D*** (black traces). Stimulus artifacts were blanked for visibility; the time of stimulation is indicated with a vertical line. ***E***, ***F***, Inward currents elicited by γ frequency train stimulation (50 Hz) of neuronal fibers in two OPCs held at −70 mV at PN8 (***E***) and PN27 (***F***), in the presence of antagonists. Stimulus artifacts were truncated for visibility. ***G***, Inward current evoked in an OPC by neuronal stimulation, resistant to a mixture of antagonists consisting of 10 μM NBQX, 50 μM D-AP5, 5 μM SR95531, 50 μM LY341495, 5 μM CPG55845, and 30 μM PPADS (all antagonists). ***H***, Effect of 0.5 μM TTX on currents induced by paired-pulse stimulation of neuronal fibers in an OPC held at −70 mV and recorded in the presence of 10 μM NBQX, 50 μM D-AP5, and 5 μM SR95531. Note the block of the current by TTX.

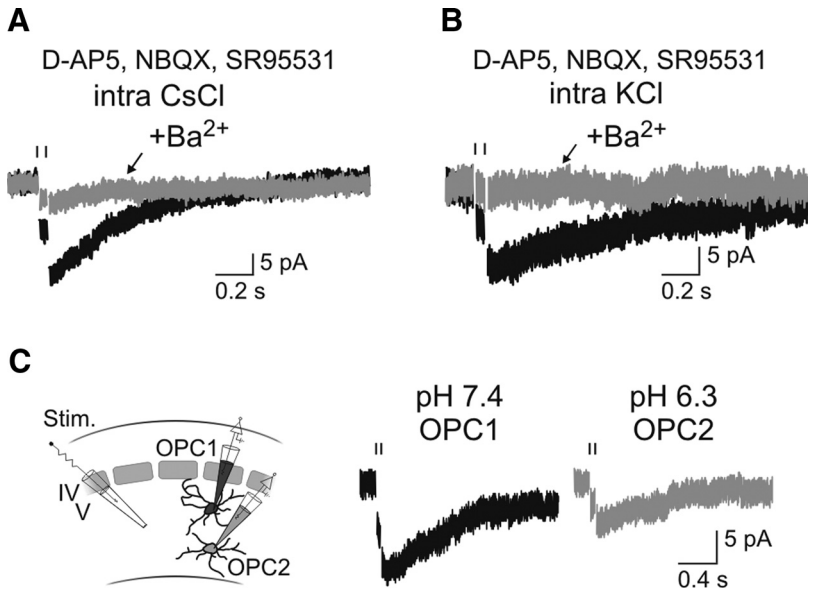

Figure 5. K^+ currents induced by neuronal activity in OPCs of 4–5PN weeks are mediated by Kir4.1 channels. ***A***, ***B***, Effect of 100 μM Ba^{2+} on inward currents resistant to antagonists and evoked by paired-pulse stimulation of neuronal fibers in OPCs held at −70 mV and recorded in CsCl-based intracellular solution (***A***) and KCl-based intracellular solution (***B***). Stimulus artifacts were blanked for visibility. A vertical line indicates the time of stimulation. Pulses were separated by 50 ms in all cases (100 μs, 40 V). ***C***, Inward currents evoked in two OPCs recorded with an intracellular solution at a pH of 7.4 (left) and of 6.3 (right) in the same slice and with the same stimulation electrode as shown in the diagram (left).

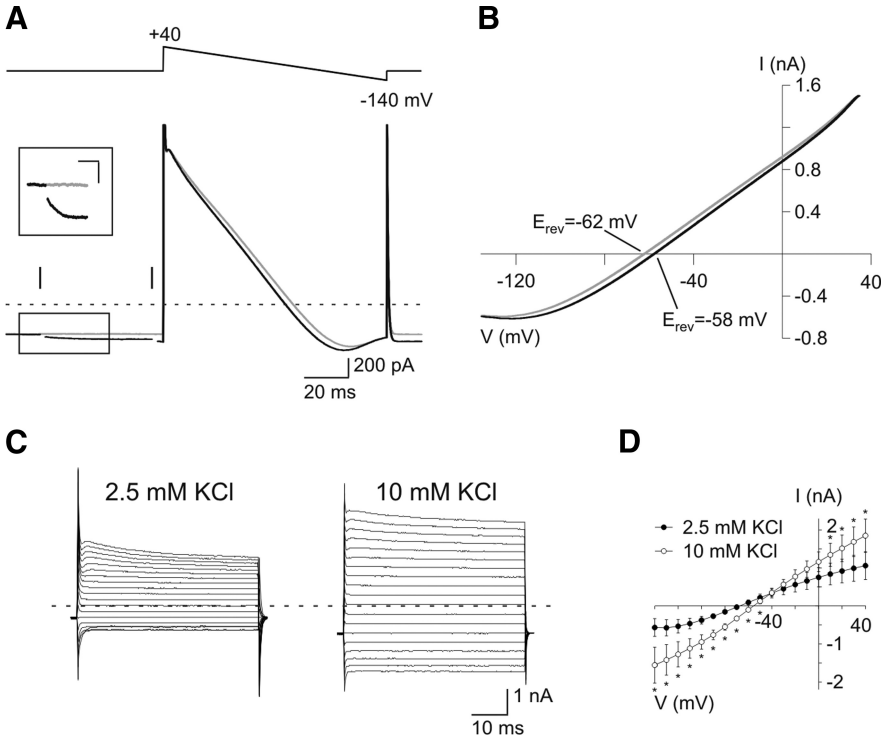

Figure 6. *I–V* curve of the persistent K^+ current evoked by neuronal stimulation. ***A***, Inward currents induced in an OPC by 100 ms ramps from +40 mV to −140 mV before the extracellular stimulation (gray trace) and at the peak of the second evoked response in the presence of 10 μM NBQX, 50 μM D-AP5, and 5 μM SR95531 (black trace; pulses separated by 50 ms; 100 μs, 40 V). The inset illustrates the persistent current evoked by paired-pulse stimulation at the first pulse. Calibration: 25 ms; 25 pA. Stimulus artifacts were blanked for visibility. A vertical line indicates the time of stimulation; a hyphenated gray line indicates zero current. ***B***, Mean *I–V* curves obtained with ramps before the stimulation (gray trace) and at the peak of the second evoked response (black trace; $n = 5$). ***C***, Effect of bath application of an increase in $[K^+]_o$ from 2.5 to 10 mM on an adult OPC held at −90 mV and recorded with the CsCl-based intracellular solution. ***D***, Comparison of mean steady-state *I–V* curves in control and after application of high $[K^+]_o$ shows an increase of induced currents and a shift in E_{rev} of -8.7 ± 2.3 mV ($p < 0.05$; $n = 6$). *$p < 0.05$.

charges while applying the same depolarizing current pulse (Fig. 7*H*,*I*). In four simultaneous recordings, the evoked current observed in the OPCs during action potential discharges was completely abolished when the neuron did not fire during current injection, confirming that neuronal action potentials are necessary to elicit a response in the OPC (-2.3 ± 1.1 pA vs 0.1 ± 0.1 pA). In addition, this current was inhibited by 100 μM Ba^{2+}, indicating that stimulation of a single neuron induces K^+ currents in OPCs through Kir4.1 channels that reflects neuronal K^+ efflux during action potential discharges (86.3 ± 8.4% of block, $n = 6$; $p < 0.05$; Fig. 7*D*,*F*). It is noteworthy that the frequency of discharge of recorded neurons remained unchanged in the presence of 100 μM Ba^{2+} (28.1 ± 6.4 Hz and 30.0 ± 6.9 Hz in control and Ba^{2+}, respectively; $p > 0.05$; $n = 6$; Fig. 7*B*,*D*, upper traces).

Altogether, our results show a novel form of unitary neuron–OPC connections that allows adult OPCs to sense finely and reliably $[K^+]_o$ increases through Kir4.1 channels during physiological activity of a single nearby neuron.

Discussion

In this report, we demonstrated that Kir4.1 channels are upregulated in cortical OPCs after the 2PN week (i.e., during their massive differentiation into oligodendrocytes) (Baracskay et al., 2002). The emergence of this conductance allows the majority of OPCs to sense local K^+ increases induced by neuronal activity, conferring to these cells a new functional property in the mature neuronal network. This novel neuron-to-OPC signaling mechanism does not rely on neurotransmitter release and is robust at a single-cell level as demonstrated by unitary neuron–OPC connections mediated by Kir4.1 channels. Astrocytes are also known to detect neuronal-induced K^+ increases through Kir4.1 channels (De Saint Jan and Westbrook, 2005; Djukic et al., 2007), but it is unknown whether they detect $[K^+]_o$ changes as locally as OPCs (i.e., upon a single neuron stimulation).

Kir channels are known to be upregulated in OPCs during postnatal development, but their expression is thought to remain low and reach high levels only in differentiated oligodendrocytes (Sontheimer et al., 1989; Berger et al., 1991; Neusch et al., 2001). However, most functional work on Kir channels of OPCs has been done either in culture or in acute slices of animals younger than four postnatal weeks (i.e., in conditions where these channels

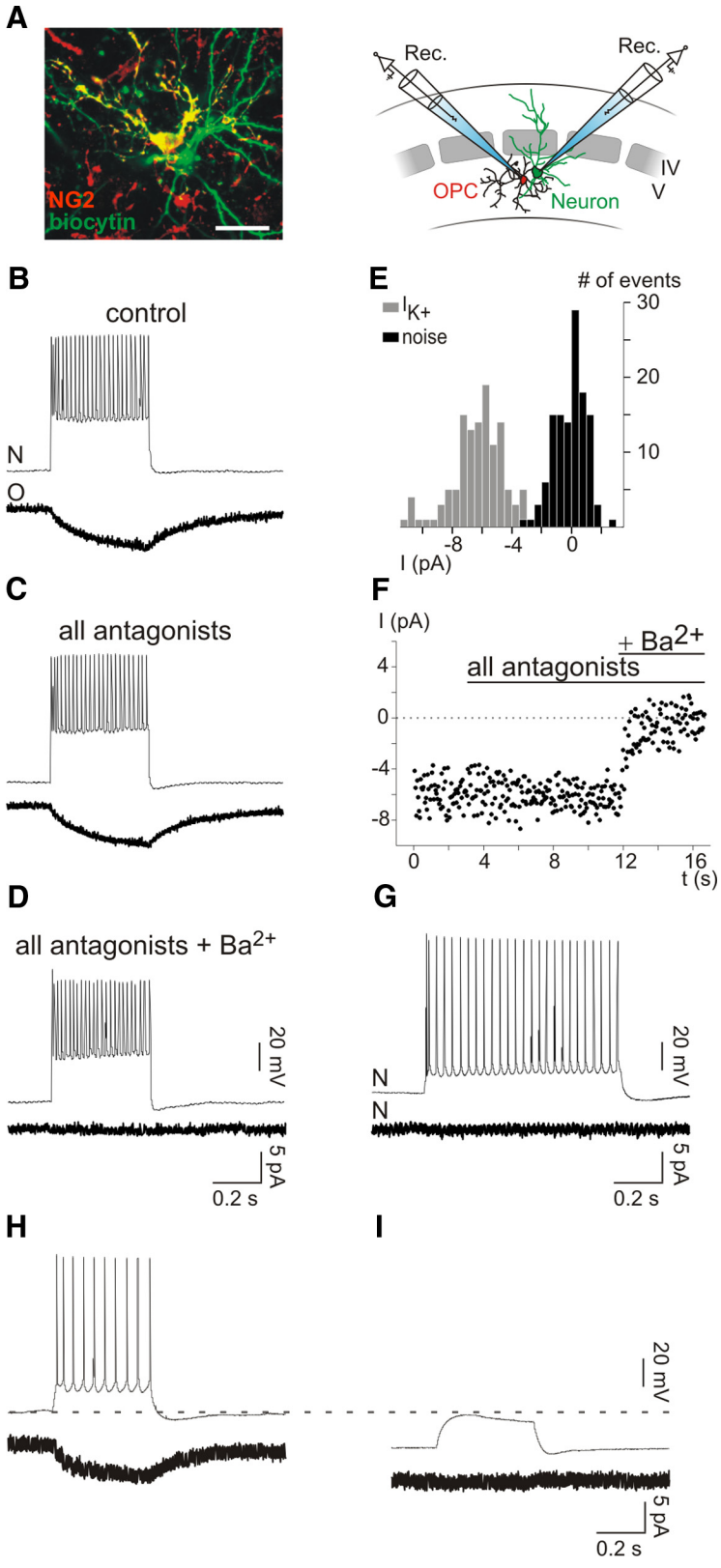

Figure 7. Single neuron stimulation induces Kir4.1-mediated K^+ currents in individual OPCs. ***A***, Confocal image of a neuron (green) and an $NG2^+$ OPC (yellow) simultaneously recorded in whole-cell configuration with intracellular solutions containing biocytin (left; stack of 17 *z* sections, each 1 μm; see Materials and Methods). The amplitude of the current elicited in this OPC by single neuron stimulation was −2.93 pA. Scale bar, 20 μm. A schematic representation of simultaneous neuron–OPC recordings is also shown (right). ***B–D***, Simultaneous recording of a neuron held at −70 mV in current clamp and an OPC held at −90 mV in voltage clamp in control (***B***), in the presence of a mixture of ionotropic and metabotropic receptor antagonists (***C***), and after bath application of 100 μM Ba^{2+} (***D***). The mixture of antagonists consists of 10 μM NBQX, 50 μM D-AP5, 5 μM SR95531, 50 μM LY341495, 5 μM CPG55845, and 30 μM PPADS. Note the lack of effect of the antagonists and the complete block of the induced current by Ba^{2+}. The train of action potentials in the recorded neuron was obtained by applying a 400 ms pulse of 400 pA, each 3 s. Only a single representative train of discharge is illustrated in each condition. Current traces of OPCs are averages of 122, 117, and 68 responses. ***E***, Amplitude distributions of the noise of the trace (black) and of the K^+ current (gray) of the recorded OPC in control conditions ($p < 0.001$). ***F***, Time course of the experiment of the same neuron–OPC simultaneous recording. ***G***, Simultaneous recording of a neuron held at −70 mV in current clamp and another neuron held at −90 mV in voltage clamp. The train of action potentials in the neuron (top) is obtained by applying 800 ms pulse of 200 pA. Note the lack of induced current in the other neuron (bottom). The current trace is an average of 37 sweeps. ***H***, ***I***, Simultaneous recording of a neuron held at −65 mV (***H***) and −90 mV (***I***) in current clamp and an OPC held at −90 mV in voltage clamp. Note that the hyperpolarization of the neuron abolishes both action potential discharges upon the same current injection and the evoked current in the OPC. The current traces are an average 51 (***H***) and 49 (***I***) sweeps.

probably do not attain their maximal expression). Although Kir4.1 channels have already been demonstrated in OPCs, only a weak expression was reported in these cells (Schroder et al., 2002; Tang et al., 2009). We showed here that expression levels of Kir4.1 channels progressively increase in most OPCs during postnatal development of the barrel cortex, conferring a linear *I–V* relationship on adult cells (Fig. 1*F*,*I*). This linear phenotype results from the weak rectification displayed by native Kir4.1 channels in physiological K^+ concentrations (Kucheryavykh et al., 2007; Seifert et al., 2009; Hibino et al., 2010). Interestingly, most of the linear *I–V* curve of astrocytes also depends on the expression of Kir4.1 channels (Djukic et al., 2007; Seifert et al., 2009). However, OPCs and astrocytes differ in that the later express functional two-pore domain K^+ channels TREK1 and probably TWIK1 (Seifert et al., 2009; Zhou et al., 2009).

Whereas voltage-gated K^+ channels expressed by OPCs play a key role during cell proliferation (Sontheimer et al., 1989; Gallo et al., 1996; Chittajallu et al., 2002), the function of Kir channels in these cells has not been well defined. Recent studies on knock-out Kir4.1 channels demonstrated that the deletion of these channels in glial cells was associated to an early lethality caused by a severe hypomyelinating phenotype (Neusch et al., 2001; Djukic et al., 2007). This has suggested that Kir4.1 channels play a role in OPC differentiation. However, the percentage of complex glia (presumably OPCs) decreases 11-fold in PN5–10 knock-out mice (Djukic et al., 2007) when functional Kir channels are poorly expressed in these cells (Fig. 1*C*) (Kressin et al., 1995). Con-

sequently, the precocious loss of progenitors probably results from an indirect effect of Kir4.1 channel deletion in other cell types, such as astrocytes, rather than from a direct effect on OPC maturation. A reduced pool of OPCs in early development is probably a major cause of hypomyelination in Kir4.1 channel knock-out mice, although a default in linear progression from preoligodendrocytes to myelinating oligodendrocytes in a successive postnatal stage may also play a role.

Interestingly, Kir4.1 channels are found almost exclusively in glial cells (Poopalasundaram et al., 2000; Higashi et al., 2001; Tang et al., 2009). The two predominant functions of these channels described so far are as follows: (1) to set the resting membrane potential and (2) to regulate $[K^+]_o$ during neuronal activity (Kofuji et al., 2000; Higashi et al., 2001; Neusch et al., 2006). Kir4.1 channels contribute to set the resting membrane potential of adult OPCs because we observed that their expression is accompanied by a more hyperpolarized resting membrane potential, and its block by different agents depolarizes the cells. Our observations showing that Kir4.1-mediated K^+ currents in adult OPCs occur upon the stimulation of neuronal fibers also suggests that neuronal activity control transient changes in the membrane potential of OPCs. Indeed, we found that γ frequency train stimulations, in the presence of AMPA, NMDA, and GABA receptor antagonists, evoked a Kir4.1-mediated current of 208 pA in adult OPCs (Fig. 4*F*). Considering that these cells have an input resistance of 70 MΩ, the current evoked by γ frequency neuronal activity should lead to a depolarization of 15 mV. It is known that whisker activation in rodents elicits the synchronization of neural ensembles at the γ frequency in the barrel cortex (Ahissar and Vaadia, 1990; Jones and Barth, 1997). Our results raises the possibility that $[K^+]_o$ increases, resulting from neuronal network oscillations, depolarize adult OPCs in the barrel cortex. The depolarizing effect of K^+ probably accumulates with that induced by activation of ligand-gated receptors during neurotransmitter release.

As a weakly inwardly rectifying conductance allowing the flow of inward and outward currents, Kir4.1 channels are suited to regulate local $[K^+]_o$ increases resulting from neuronal activity. Indeed, these channels can mediate both K^+ entry at sites of maximal accumulation and K^+ exit at sites of lower concentration. This mechanism of K^+ removal requires that cells in charge of K^+ redistribution have a high permeability for this ion and a resting membrane potential close to E_{rev} for K^+. Astrocytes are considered major players of K^+ buffering because K^+ can enter the astrocytic syncytium formed by gap junctions in a region of high neuronal activity and leave it in a remote region, the so-called spatial K^+ buffering (Orkand et al., 1966). However, this form of K^+ buffering is not sufficient to maintain $[K^+]_o$ at low levels, and it works most probably in concert with other auxiliary mechanisms (Newman et al., 1984; Ballanyi et al., 1987; Kofuji and Newman, 2004; Wallraff et al., 2006). This is particularly true for adult animals where volumes of extracellular space decrease with age in correlation with the myelination process and generate more considerable changes in $[K^+]_o$ (Chvatal et al., 1997). The presence of Kir4.1 channels in adult OPCs raises the possibility that these cells contribute to take up the K^+ released by nearby active neurons at sites that are not reached by astrocytic processes. Consistent with this, OPCs sense $[K^+]_o$ rises generated by a single neuronal firing, suggesting that astrocytes do not intervene between the neuron and the OPC to absorb K^+. Indeed, it is known that OPCs in the mature brain are closely associated with neurons by forming intimate contacts with neuronal somata, dendritic trees, and nodes of Ranvier (Butt et al., 2005). They are thus ideally located to sense K^+ increases and possibly remove the excess of K^+ caused by neuronal K^+ efflux at specific sites devoid of astrocytes. Because cortical OPCs are not connected by gap junctions (Vélez-Fort et al., 2010), one possibility is that this ion is temporarily sequestered at specific sites and then released back either to another site of the extracellular space reached by the cell or to blood vessels. Indeed, single OPCs project their processes to distinct cell layers and to blood vessels (Butt et al., 2005). This role could not be accomplished by young OPCs because they do not respond to neuronal activity through Kir4.1 channels.

In conclusion, our data reconcile a developmental upregulation of a K^+ channel with the capacity of adult OPCs to sense fine changes of local $[K^+]_o$ increases induced by physiological neuronal activity. They thus add a further complexity, previously unsuspected, to the mechanisms used by OPCs to detect neuronal activity in mature gray matter. This new functional property of adult OPCs in the neuronal network suggests that these cells might play a role in K^+ uptake in the mature healthy brain and, beyond their large abundance, the postnatal gain of physiological properties in neuronal networks support the view that these cells are not progenitors only.

References

Ahissar E, Vaadia E (1990) Oscillatory activity of single units in a somatosensory cortex of an awake monkey and their possible role in texture analysis. Proc Natl Acad Sci U S A 87:8935–8939. CrossRef Medline

Angulo MC, Lambolez B, Audinat E, Hestrin S, Rossier J (1997) Subunit composition, kinetic, and permeation properties of AMPA receptors in single neocortical nonpyramidal cells. J Neurosci 17:6685–6696. Medline

Angulo MC, Staiger JF, Rossier J, Audinat E (1999) Developmental synaptic changes increase the range of integrative capabilities of an identified excitatory neocortical connection. J Neurosci 19:1566–1576. Medline

Ballanyi K, Grafe P, ten Bruggencate G (1987) Ion activities and potassium uptake mechanisms of glial cells in guinea-pig olfactory cortex slices. J Physiol 382:159–174. Medline

Baracskay KL, Duchala CS, Miller RH, Macklin WB, Trapp BD (2002) Oligodendrogenesis is differentially regulated in gray and white matter of jimpy mice. J Neurosci Res 70:645–654. CrossRef Medline

Berger T, Schnitzer J, Kettenmann H (1991) Developmental changes in the membrane current pattern, K+ buffer capacity, and morphology of glial cells in the corpus callosum slice. J Neurosci 11:3008–3024. Medline

Bergles DE, Roberts JD, Somogyi P, Jahr CE (2000) Glutamatergic synapses on oligodendrocyte precursor cells in the hippocampus. Nature 405:187–191. CrossRef Medline

Butt AM, Hamilton N, Hubbard P, Pugh M, Ibrahim M (2005) Synantocytes: the fifth element. J Anat 207:695–706. CrossRef Medline

Cahoy JD, Emery B, Kaushal A, Foo LC, Zamanian JL, Christopherson KS, Xing Y, Lubischer JL, Krieg PA, Krupenko SA, Thompson WJ, Barres BA (2008) A transcriptome database for astrocytes, neurons, and oligodendrocytes: a new resource for understanding brain development and function. J Neurosci 28:264–278. CrossRef Medline

Chittajallu R, Chen Y, Wang H, Yuan X, Ghiani CA, Heckman T, McBain CJ, Gallo V (2002) Regulation of Kv1 subunit expression in oligodendrocyte progenitor cells and their role in G_1/S phase progression of the cell cycle. Proc Natl Acad Sci U S A 99:2350–2355. CrossRef Medline

Chvátal A, Berger T, Vorísek I, Orkand RK, Kettenmann H, Syková E (1997) Changes in glial K+ currents with decreased extracellular volume in developing rat white matter. J Neurosci Res 49:98–106. CrossRef Medline

Dawson MR, Polito A, Levine JM, Reynolds R (2003) NG2-expressing glial progenitor cells: an abundant and widespread population of cycling cells in the adult rat CNS. Mol Cell Neurosci 24:476–488. CrossRef Medline

De Saint Jan D, Westbrook GL (2005) Detecting activity in olfactory bulb glomeruli with astrocyte recording. J Neurosci 25:2917–2924. CrossRef Medline

De Biase LM, Nishiyama A, Bergles DE (2010) Excitability and synaptic communication within the oligodendrocyte lineage. J Neurosci 30:3600–3611. CrossRef Medline

Djukic B, Casper KB, Philpot BD, Chin LS, McCarthy KD (2007) Condi-

tional knock-out of Kir4.1 leads to glial membrane depolarization, inhibition of potassium and glutamate uptake, and enhanced short-term synaptic potentiation. J Neurosci 27:11354–11365. CrossRef Medline

Gallo V, Zhou JM, McBain CJ, Wright P, Knutson PL, Armstrong RC (1996) Oligodendrocyte progenitor cell proliferation and lineage progression are regulated by glutamate receptor-mediated K+ channel block. J Neurosci 16:2659–2670. Medline

Heinemann U, Lux HD (1977) Ceiling of stimulus induced rises in extracellular potassium concentration in the cerebral cortex of cat. Brain Res 120:231–249. CrossRef Medline

Hibino H, Inanobe A, Furutani K, Murakami S, Findlay I, Kurachi Y (2010) Inwardly rectifying potassium channels: their structure, function, and physiological roles. Physiol Rev 90:291–366. CrossRef Medline

Higashi K, Fujita A, Inanobe A, Tanemoto M, Doi K, Kubo T, Kurachi Y (2001) An inwardly rectifying K(+) channel, Kir4.1, expressed in astrocytes surrounds synapses and blood vessels in brain. Am J Physiol Cell Physiol 281:C922–C931. Medline

Jones MS, Barth DS (1997) Sensory-evoked high-frequency (γ-band) oscillating potentials in somatosensory cortex of the unanesthetized rat. Brain Res 768:167–176. CrossRef Medline

Káradóttir R, Cavelier P, Bergersen LH, Attwell D (2005) NMDA receptors are expressed in oligodendrocytes and activated in ischaemia. Nature 438:1162–1166. CrossRef Medline

Kofuji P, Newman EA (2004) Potassium buffering in the central nervous system. Neuroscience 129:1045–1056. CrossRef Medline

Kofuji P, Ceelen P, Zahs KR, Surbeck LW, Lester HA, Newman EA (2000) Genetic inactivation of an inwardly rectifying potassium channel (Kir4.1 subunit) in mice: phenotypic impact in retina. J Neurosci 20:5733–5740. Medline

Kressin K, Kuprijanova E, Jabs R, Seifert G, Steinhäuser C (1995) Developmental regulation of Na+ and K+ conductances in glial cells of mouse hippocampal brain slices. Glia 15:173–187. CrossRef Medline

Kucheryavykh YV, Pearson WL, Kurata HT, Eaton MJ, Skatchkov SN, Nichols CG (2007) Polyamine permeation and rectification of Kir4.1 channels. Channels (Austin) 1:172–178. Medline

Kukley M, Capetillo-Zarate E, Dietrich D (2007) Vesicular glutamate release from axons in white matter. Nat Neurosci 10:311–320. CrossRef Medline

Lesage F, Guillemare E, Fink M, Duprat F, Lazdunski M, Romey G, Barhanin J (1996) TWIK-1, a ubiquitous human weakly inward rectifying K+ channel with a novel structure. EMBO J 15:1004–1011. Medline

Lotshaw DP (2007) Biophysical, pharmacological, and functional characteristics of cloned and native mammalian two-pore domain K+ channels. Cell Biochem Biophys 47:209–256. CrossRef Medline

Maldonado PP, Vélez-Fort M, Angulo MC (2011) Is neuronal communication with NG2 cells synaptic or extrasynaptic? J Anat 219:8–17. CrossRef Medline

Mangin JM, Kunze A, Chittajallu R, Gallo V (2008) Satellite NG2 progenitor cells share common glutamatergic inputs with associated interneurons in the mouse dentate gyrus. J Neurosci 28:7610–7623. CrossRef Medline

Morales B, Choi SY, Kirkwood A (2002) Dark rearing alters the development of GABAergic transmission in visual cortex. J Neurosci 22:8084–8090. Medline

Neusch C, Rozengurt N, Jacobs RE, Lester HA, Kofuji P (2001) Kir4.1 potassium channel subunit is crucial for oligodendrocyte development and in vivo myelination. J Neurosci 21:5429–5438. Medline

Neusch C, Papadopoulos N, Müller M, Maletzki I, Winter SM, Hirrlinger J, Handschuh M, Bähr M, Richter DW, Kirchhoff F, Hülsmann S (2006) Lack of the Kir4.1 channel subunit abolishes K+ buffering properties of astrocytes in the ventral respiratory group: impact on extracellular K+ regulation. J Neurophysiol 95:1843–1852. CrossRef Medline

Newman EA, Frambach DA, Odette LL (1984) Control of extracellular potassium levels by retinal glial cell K^+ siphoning. Science 225:1174–1175. CrossRef Medline

Nie X, Arrighi I, Kaissling B, Pfaff I, Mann J, Barhanin J, Vallon V (2005) Expression and insights on function of potassium channel TWIK-1 in mouse kidney. Pflugers Arch 451:479–488. CrossRef Medline

Orkand RK, Nicholls JG, Kuffler SW (1966) Effect of nerve impulses on the membrane potential of glial cells in the central nervous system of amphibia. J Neurophysiol 29:788–806. Medline

Patel AJ, Honoré E, Lesage F, Fink M, Romey G, Lazdunski M (1999) Inhalational anesthetics activate two-pore-domain background K^+ channels. Nat Neurosci 2:422–426. CrossRef Medline

Pessia M, Imbrici P, D'Adamo MC, Salvatore L, Tucker SJ (2001) Differential pH sensitivity of Kir4.1 and Kir4.2 potassium channels and their modulation by heteropolymerisation with Kir5.1. J Physiol 532:359–367. CrossRef Medline

Poopalasundaram S, Knott C, Shamotienko OG, Foran PG, Dolly JO, Ghiani CA, Gallo V, Wilkin GP (2000) Glial heterogeneity in expression of the inwardly rectifying K(+) channel, Kir4.1, in adult rat CNS. Glia 30:362–372. CrossRef Medline

Richardson WD, Young KM, Tripathi RB, McKenzie I (2011) NG2-glia as multipotent neural stem cells: fact or fantasy? Neuron 70:661–673. CrossRef Medline

Sah P, Faber ES (2002) Channels underlying neuronal calcium-activated potassium currents. Prog Neurobiol 66:345–353. CrossRef Medline

Salami M, Itami C, Tsumoto T, Kimura F (2003) Change of conduction velocity by regional myelination yields constant latency irrespective of distance between thalamus and cortex. Proc Natl Acad Sci U S A 100:6174–6179. CrossRef Medline

Schröder W, Seifert G, Hüttmann K, Hinterkeuser S, Steinhäuser C (2002) AMPA receptor-mediated modulation of inward rectifier K+ channels in astrocytes of mouse hippocampus. Mol Cell Neurosci 19:447–458. CrossRef Medline

Seifert G, Hüttmann K, Binder DK, Hartmann C, Wyczynski A, Neusch C, Steinhäuser C (2009) Analysis of astroglial K+ channel expression in the developing hippocampus reveals a predominant role of the Kir4.1 subunit. J Neurosci 29:7474–7488. CrossRef Medline

Sontheimer H, Trotter J, Schachner M, Kettenmann H (1989) Channel expression correlates with differentiation stage during the development of oligodendrocytes from their precursor cells in culture. Neuron 2:1135–1145. CrossRef Medline

Su S, Ohno Y, Lossin C, Hibino H, Inanobe A, Kurachi Y (2007) Inhibition of astroglial inwardly rectifying Kir4.1 channels by a tricyclic antidepressant, nortriptyline. J Pharmacol Exp Ther 320:573–580. CrossRef Medline

Tang X, Taniguchi K, Kofuji P (2009) Heterogeneity of Kir4.1 channel expression in glia revealed by mouse transgenesis. Glia 57:1706–1715. CrossRef Medline

Tang X, Schmidt TM, Perez-Leighton CE, Kofuji P (2010) Inwardly rectifying potassium channel Kir4.1 is responsible for the native inward potassium conductance of satellite glial cells in sensory ganglia. Neuroscience 166:397–407. CrossRef Medline

Taverna S, Tkatch T, Metz AE, Martina M (2005) Differential expression of TASK channels between horizontal interneurons and pyramidal cells of rat hippocampus. J Neurosci 25:9162–9170. CrossRef Medline

Tucker SJ, Imbrici P, Salvatore L, D'Adamo MC, Pessia M (2000) pH dependence of the inwardly rectifying potassium channel, Kir5.1, and localization in renal tubular epithelia. J Biol Chem 275:16404–16407. CrossRef Medline

Vélez-Fort M, Audinat E, Angulo MC (2009) Functional α 7-containing nicotinic receptors of NG2-expressing cells in the hippocampus. Glia 57:1104–1114. CrossRef Medline

Vélez-Fort M, Maldonado PP, Butt AM, Audinat E, Angulo MC (2010) Postnatal switch from synaptic to extrasynaptic transmission between interneurons and NG2 cells. J Neurosci 30:6921–6929. CrossRef Medline

Wallraff A, Köhling R, Heinemann U, Theis M, Willecke K, Steinhäuser C (2006) The impact of astrocytic gap junctional coupling on potassium buffering in the hippocampus. J Neurosci 26:5438–5447. CrossRef Medline

Zhou M, Schools GP, Kimelberg HK (2006) Development of GLAST(+) astrocytes and NG2(+) glia in hippocampus CA1: mature astrocytes are electrophysiologically passive. J Neurophysiol 95:134–143. CrossRef Medline

Zhou M, Xu G, Xie M, Zhang X, Schools GP, Ma L, Kimelberg HK, Chen H (2009) TWIK-1 and TREK-1 are potassium channels contributing significantly to astrocyte passive conductance in rat hippocampal slices. J Neurosci 29:8551–8564. CrossRef Medline

Ziskin JL, Nishiyama A, Rubio M, Fukaya M, Bergles DE (2007) Vesicular release of glutamate from unmyelinated axons in white matter. Nat Neurosci 10:321–330. CrossRef Medline